

PCCP

Accepted Manuscript



This is an *Accepted Manuscript*, which has been through the Royal Society of Chemistry peer review process and has been accepted for publication.

Accepted Manuscripts are published online shortly after acceptance, before technical editing, formatting and proof reading. Using this free service, authors can make their results available to the community, in citable form, before we publish the edited article. We will replace this *Accepted Manuscript* with the edited and formatted *Advance Article* as soon as it is available.

You can find more information about *Accepted Manuscripts* in the [Information for Authors](#).

Please note that technical editing may introduce minor changes to the text and/or graphics, which may alter content. The journal's standard [Terms & Conditions](#) and the [Ethical guidelines](#) still apply. In no event shall the Royal Society of Chemistry be held responsible for any errors or omissions in this *Accepted Manuscript* or any consequences arising from the use of any information it contains.

Molecular Dynamics simulations for designing biomimetic pores based on internally functionalized self-assembling α,γ -peptide nanotubes

Martín Calvelo^a, Saulo Vázquez^b, Rebeca García-Fandiño^{a,}*

^aDepartment of Organic Chemistry and ^bDepartment of Physical Chemistry, Center for Research in Biological Chemistry and Molecular Materials, Campus Vida, Santiago de Compostela University, E-15782 Santiago de Compostela, (Spain)

Corresponding author e-mail: rebeca.garcia.fandino@usc.es

Abstract

A Molecular Dynamics study on internally functionalized peptide nanotubes composed of α - and γ -amino acids self-assembled in lipid bilayers is presented. One of the main advantages of peptide nanotubes composed of γ -amino acids is that the properties of their inner cavities can be tuned by introducing different functions on the β -carbon of the γ -amino acid. In the work described here we studied the effect of the presence of different numbers of hydroxyl groups in different positions in the lumen of these channels when they are inserted into a lipid bilayer and assessed how they affect the structural and dynamical behavior of the modified peptide nanotubes as well as the transmembrane transport of different ions. The results provided atomic information about the effect of polar groups on

the dynamical, structural and transport properties of this type of peptidic channel upon insertion into lipid bilayers, projecting a promising future for their use as biomimetic channels when properly inner-derivatized. Furthermore, the chemical versatility of the hydroxyl groups in the lumen of the peptide nanotubes would enable appealing applications for these channels, such as a controlled method for the activation/inactivation of the transmembrane transport along the nanopore.

Keywords Self-assembling, Peptide Nanotubes, Biomimetic channels, Molecular Dynamics, Ion transport, Lumen functionalization

Introduction

The selective and effective passage of ions and molecules through the cell membrane is a process that is of vital importance to cellular function. Of all the available transport processes, ion channels and pores stand out due to their high selectivity and efficiency in discriminating and transporting ions or molecules across lipid bilayers.¹ Attempts to capture the fundamental features used by Nature to achieve this formidable task have resulted in the design and construction of a number of artificial ion channels and carriers.² The design of biomimetic systems is of prime importance to understand the fundamental operations of natural channels, as well as in the technological development of biosensors, catalysts, drug delivery systems, antimicrobial agents and functional materials of use in the bio- and nanotechnology fields.³

Most of the biomimetic approaches have included rigid amphiphilic rods that aggregate to form a central opening,⁴ macrocyclic ion-conducting ring systems with membrane-spanning ‘tails’,⁵ linear polymers that fold into a helix through which ions can travel,⁶ or stackable macrocyclic rings that form ion-transporting cylinders.⁷ It has been demonstrated that peptide nanotubes can also act as ion channels.^{2e} In 1994, Ghadiri et al. proposed the formation of ion channels through the self-assembly of cyclic peptides (CPs). Studies carried out with the cyclic peptide $c\text{-}[L\text{-Gln-}D\text{-Leu-(}L\text{-Trp-}D\text{-Leu-)}_3]$ highlighted that

they inserted into lipid bilayers and were able to form transmembrane pores that transported more than 10^7 K^+ and Na^+ ions per second, a rate similar to or greater than that of gramicidin A or amphotericin B.⁸ Further studies demonstrated that hydrophobic CPs self-assemble in the membrane with their central axis tilted by 70 degrees with respect to the lipid bilayer.⁹ From these studies it can be inferred that the nanotube orientation in the membrane depends on the CP sequence, where hydrophobic CPs form transmembrane nanotubes (i.e., perpendicular to the membrane), while amphipathic CPs orient parallel to the lipid bilayers. β -CPs have also been studied as molecular precursors of ion channels as they form pores in lipid bilayers and transport K^+ at a rate comparable to that of *D,L*- α -cyclooctapeptides (1.9×10^7 ions per second), suggesting that this type of compound could be used as biological sensors or in drug delivery (Figure 1).¹⁰

Although Self assembling Cyclic Peptide Nanotube (SCPN)-mediated transport has been widely studied and applied, there is still a great deal of work to be done in this field. Efforts should now focus on lumen functionalization and topological adjustment of the nanotube assembly.¹¹ The structural features of the previously described *D,L*- α -CP and β^3 -CP flat-shaped rings inherently inhibited any further chemical modification of the inner cavities in the corresponding nanotubes. The key design feature to overcome this drawback, while maintaining the same self-assembly driven principles of SCPNs, emerged from CPs bearing γ -aminocycloalkanecarboxylic acids (γ -Aca), such as (1*R*,3*S*)-3-aminocyclohexanecarboxylic acid (*D*- γ -Ach) or (1*R*,3*S*)-3-aminocyclopentanecarboxylic acid (*D*- γ -Acp) combined with α -Aas of appropriate chirality, such as α,γ -CP, $3\alpha,\gamma$ -CP, or even γ -CP.¹² The most studied were the α,γ -CP that structurally are quite unique because their formation involves two different sets of β -sheet-like H-bonds: one exclusively between the NH and C=O groups of the γ -amino acids (γ - γ interaction, Figure 1), all of which are projected in the same direction, and the other between the same groups of the α -amino acids (α - α bonding, Figure 1), which are oriented towards the opposite face. The use of γ -Acas imparts additional properties on the nanotube; for example, while almost all of the cyclic peptide nanotubes

that have been developed so far have hydrophilic inner surfaces, thus allowing the permeation of only polar molecules, in the γ -Acas-containing SCPN systems the C2 methylene group of each cycloalkane moiety is projected into the lumen of the cylindrical structure to generate a partially hydrophobic cavity. Furthermore, the cavity properties can be modulated by simple chemical modification of the β -carbon of the cyclic γ -Acas and this allows, in principle, finer control of the transport properties of a very wide range of molecules in the nanotube. The use of non-covalent synthetic processes to build, through molecular self-assembling processes, peptide nanotubes with novel properties in an efficient way allows their formation in a variety of conditions with a precise control of their internal diameter. The simplicity with which the external surface properties of α,γ -SCPNs can be modulated by simply selecting the appropriate amino acid sequence in the cyclic peptides, together with the great capability of their lumen functionalization and topological adjustment of the nanotube assembly, make these systems very good candidates for being used as biomimetic channels. This biomimetic approach could allow the study of biological pores through bottom-up engineering approaches, whereby constituent components can be investigated outside the complex cellular environment.

Recently, we reported that α,γ -SCPNs can also insert into a lipid bilayer and conduct ions.¹³ An octameric α,γ -CP with an internal diameter of 7.5 Å (c-[L-Gln-D- γ -Ach-(L-Trp-D- γ -Ach)₃]) showed a transport rate in the order of 10⁷ ions/s, the mean open time was slightly shorter than that of D,L- α -CPs, and the overall ion transport efficiency was five times lower.

The first steps toward the preparation of functionalized γ -Acas have already been achieved with 4-amino-3-hydroxytetrahydrofuran-2-carboxylic acid (γ -Ahf-OH).¹⁴ ¹H NMR experiments on the tetrameric model cyclo-[D-Leu-(2S,3R)- γ -Ahf-D-Tyr(Me)-(1R,3S)- γ -^{Me}N-Acp-] confirmed the adoption of the required flat conformation of the CP ring with the equatorial hydroxyl substituent pointing inwards in the ensemble. These promising results represent the first step toward the preparation of stable and ordered SCPNs with chemically functionalized lumens. The access to this new class of engineered

nanotubes will open a broad range of feasible designs and conceptual devices, such as selectivity filters for artificial ion channels, catalytic pores, receptors, or molecule containers. For example, the development of selective ion channels would address the treatment of diseases related to *channelopathies*, such as cystic fibrosis.¹⁵ Furthermore, additional knowledge of the effects of the internal functionalization of these channels would contribute to the design of artificial biomimetic nanopores that could reproduce functions of biological systems.^{16, 11b} For example, synthetic nanopores based on the permeation properties of biological channels and nanotubes that mimic the transport properties of the nuclear pore complex have been designed.^{17, 18} Besides, the formation of ion channels with a perfectly controlled diameter and functionalization (outer and inner) would allow the intratubular passage of charged biopolymer chains (DNA, RNA, mRNA) and this could facilitate, for example, their sequentiation.

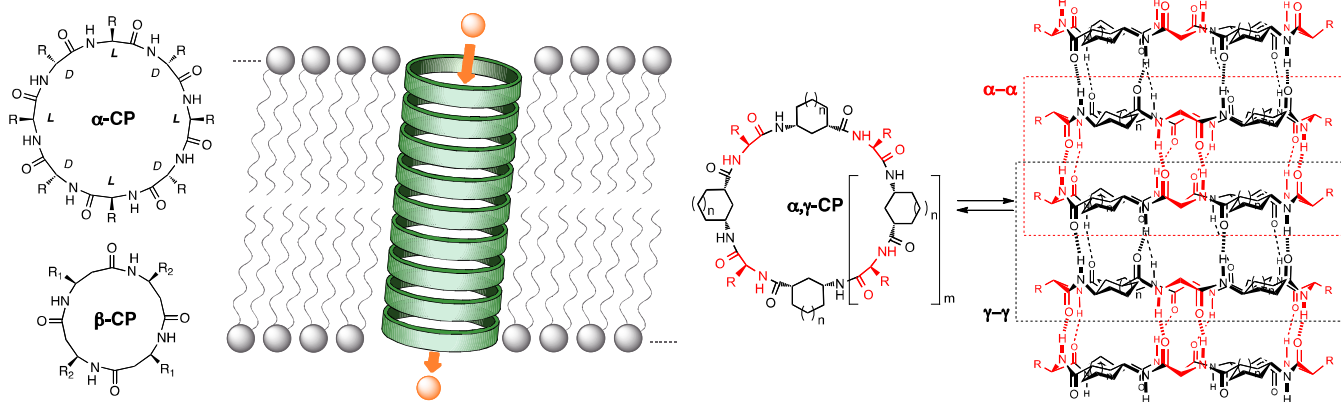


Figure 1: Model of a self-assembled peptide nanotube inserted into a lipid bilayer. Schematic diagram of SCPNs composed of α -amino acids, β -amino acids and those formed by the alternation of γ -Ach ($n=1$) or γ -Acp ($n=0$) and α -amino acids. The α - α and γ - γ H-bonding patterns are shown.

Theoretical approaches, such as computational modeling and simulations, have contributed to both our understanding of natural systems and to the design principles for engineering approaches.¹⁹ In contrast to the large amount of theoretical work on ‘classical’ D,L - α -SCPns,²⁰ very little theoretical work has been performed on α,γ -SCPns,^{13,21} and even less has been done for nanotubes derivatized in their inner cavity. Molecular Dynamics (MD) simulations are capable of acting as a virtual microscope

with high spatial and temporal resolution, and this approach could provide powerful information about the fine details of the effect that lumen functionalization of these systems has on the ion transport when they are inserted into a lipid bilayer. In this work we used MD simulations to study three different α,γ -SCPNs in which the lumen is decorated with hydroxyl groups at different positions (Figure 2). All of these systems consist of 10 units of an octameric cyclic peptide (c-[(L-Trp-D- γ -Ach-)₄]), analogous to a non-functionalized system that was previously studied experimentally and computationally,¹³ but where the equatorial hydrogen of the β -carbon of the Ach moiety is replaced by a hydroxyl group in all four γ -Aas (SCP_N_{4OH}) or in only on two opposite faced of the γ -Ach_s of the cyclic peptide [SCP_N_{2OH}(**a**) or SCP_N_{2OH}(**e**)]. In all three cases the modifications alter the hydrophilic character of the cavities in a controlled manner. The presence of two hydroxyl groups in each of the CPs that form the nanotube can lead to two possible relative orientations per two cyclic peptides, one in which the OH groups are eclipsed, they lay on top of each other [**D**_{2OH}(**e**) and **D**_{2OH}(**a**), respectively], and the other in which the OH groups are alternated with respect to those in the neighboring CPs. Although in a ten-cyclopeptides nanotubes the number of inter-subunit arrangements are very large ($2^{(n-1)}$), we have decided to carry our studies with only two models, the one in which all the hydroxylated units are aligned all along the nanotube [SCP_N_{2OH}(**e**)], and the other in which the γ -Ach_s with OH groups are alternated with respect to those in the neighboring CPs [SCP_N_{2OH}(**a**)]. The results provide atomic information about the effect of these polar groups on the dynamic, structural and transport properties of this type of peptidic channel inserted into lipid bilayers.

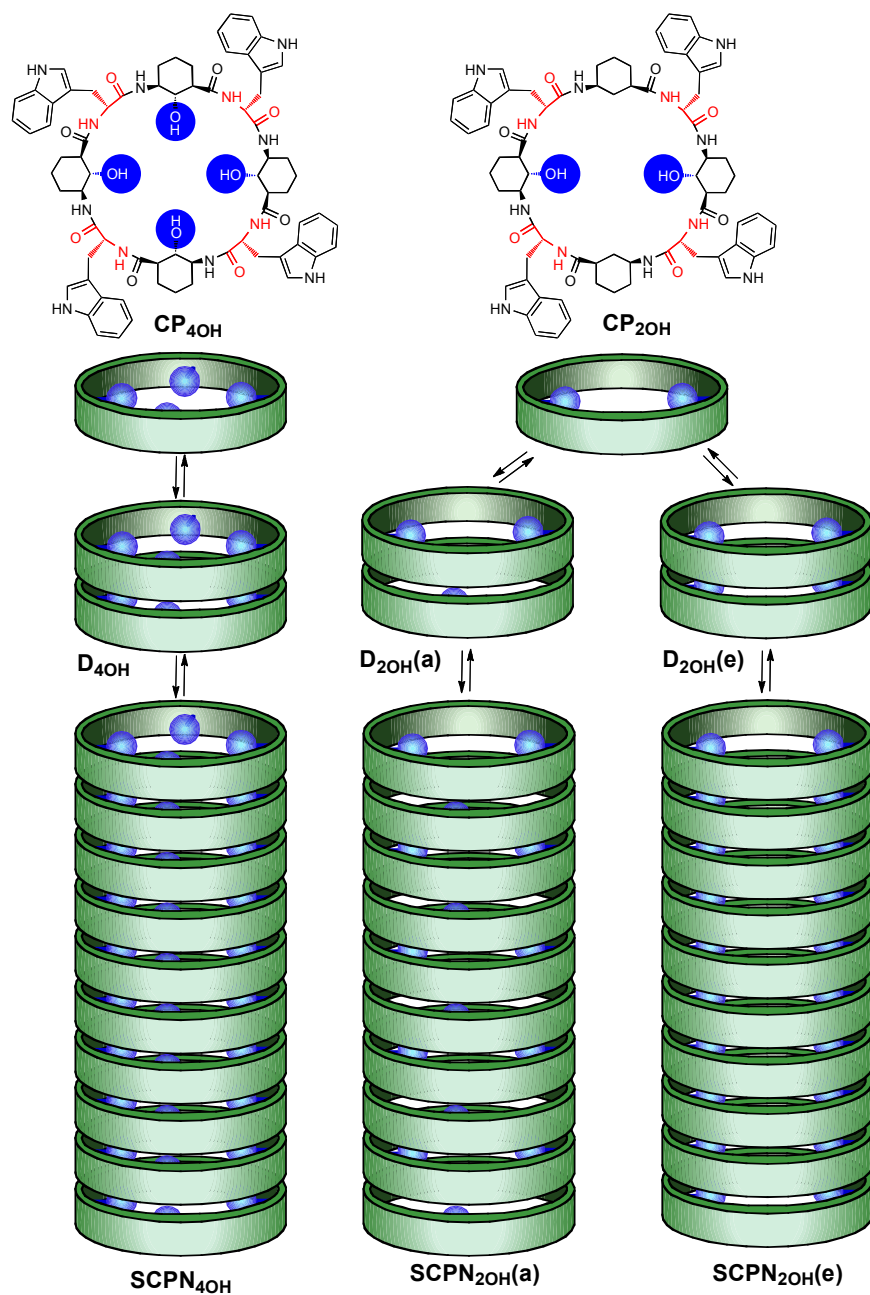


Figure 2: Schematic models of the three functionalized nanotubes studied in this work, highlighting the position of the hydroxyl groups (in blue), leading to SCPN_{4OH} from CP_{4OH} and alternated [SCPN_{2OH}(a)] or eclipsed [SCPN_{2OH}(e)] structures from the CP_{2OH}.

Experimental (methods)

The starting geometries of the cyclic peptides investigated in this work were constructed from X-ray crystallographic data of related compounds: $c\text{-}[(D\text{-Phe-}L\text{-}^{\text{Me}}N\text{-}\gamma\text{-Ach-})_4]$.²² From the structures of the

dimers, the N-methyl groups were removed and replaced by protons, the phenylalanines were substituted by tryptophan and the equatorial hydrogens of the β -carbons of the cycloalkane moieties were changed to hydroxyl groups in the corresponding γ -Achs [in all the γ -Achs for **CP_{4OH}** that forms **D_{4OH}** or in only two opposite γ -Achs for **CP_{2OH}** that gives rise to **D_{2OH(a)}** and **D_{2OH(e)}**]. The dimers were then replicated five times along the axis perpendicular to the CP planes by a distance equal to that measured between the two original CP units. The terminal CPs of the resultant nanotubes were removed in order to achieve that the first interaction in the channel will be the stronger γ - γ interaction.²³ Therefore, the resulting cyclic peptide nanotubes, **SCPN_{4OH}**, **SCPN_{2OH(e)}** and **SCPN_{2OH(a)}** are composed of ten CP units. The hydroxymethylated channel **SCPN_{4OMe}** was prepared from **SCPN_{4OH}**, replacing the hydroxyl hydrogens by methyl groups and submitted to the same simulation protocol than the other channels.

Concerning the atoms of the SCPN, RESP/6-31G(d) charges were derived as in the original AMBER force-field development, while van der Waals parameters were taken from the GAFF force-field²⁴ using standard Lorenz–Bertelot combination rules. Bonded terms were taken as those of standard peptides. The water (SPC/E)/ion combination parameters published by Joung et al.,²⁵ as implemented in AMBER10,²⁶ were used to prevent the crystallization previously reported at high concentrations with other parameter sets. The GAFF force field was used for DOPC lipids, as this approach was employed in previous studies²⁷ from which we obtained a pre-equilibrated membrane for subsequent replication. The bilayer was replicated three times in the x and y directions (or only twice in the case of the PMF calculations) and, after SCPN insertion, the complete system was solvated. Water in the hydrophobic region of the tails and also inside the SCPN was removed, so that in the first step of the simulation the channel was completely dry. The resulting systems were ionized using different salts solutions (LiCl, NaCl, KCl, CsCl and CaCl₂ at 0.5M, respectively). In this way, a total of 15 systems were prepared. The initial size of the unit cell in each case was equal to $15.1 \times 15.2 \times 6.9 \text{ nm}^3$ and contained ~555 lipids, ~476 cations and ~18000 water molecules.

The equilibrium simulations were performed with the GROMACS 4.5²⁸ Molecular Dynamics program. All systems were partially optimized, thermalized, and equilibrated, followed by unrestrained simulations for 40 ns (time step = 2 fs) for each of the systems studied. The constant pressure and temperature NPT ensemble was employed with a pressure of 1 bar controlled using a semi-isotropic Parrinello–Rahman barostat,²⁹ and a temperature of 300 K imposed by a V-rescale thermostat (Temperature coupling using velocity rescaling with a stochastic term).³⁰ The LINCS³¹ algorithm was employed to remove the bond vibrations. The Particle Mesh Ewald method³² coupled to periodic boundary conditions was used to treat the long-range electrostatics using a direct-space cutoff of 1.0 nm and a grid spacing of 0.12 nm. The van der Waals interactions were computed using PBC coupled to a spherical *cutoff* of 1.0 nm.

The potential of mean force (PMF) of the specific ion moving through each one of the investigated nanotubes was calculated using umbrella sampling. The 1D reaction pathway corresponds to the distance along the z axis of the SCPN. For umbrella sampling, the particle of interest was harmonically restrained to subsequent positions on the channel axis (with typical values of the restraining force constant of $1000 \text{ kJ mol}^{-1} \text{ nm}^{-2}$) in 100 windows of with $\Delta z = 0.05 \text{ nm}$. This restricted movement of the ion to the xy -plane while still allowing diffusion into adjacent windows. Each window was initially minimized. One MD simulation of length 2 ns was carried out for each of the 100 windows. The 100 biased distributions of z positions of the test particle were recombined and unbiased with the Weighted Histogram Analysis Method (WHAM).³³ The first 0.6 ns of each window run were discarded as equilibration time, leaving a total of 1.4 ns per window.

Data were analyzed using GROMACS and locally written code. Molecular graphic images were prepared using visual Molecular Dynamics (VMD).³⁴ The analysis of ions and water molecules inside the channels was carried out using g_count , g_flux and g_zcoord , developed for GROMACS by O. Beckstein.³⁵ A total of more than half a million computational hours were needed to complete all the calculations.

Results and Discussion

In addition to a higher hydrophilic character, the presence of the hydroxyl groups also leads to a decrease in the interior net space of the channels. The effective radii of the functionalized channels were calculated with HOLE³⁶ both before and after the MD simulation and the values were compared to that of the non-derivatized channel SCPN (Figure 3). In all cases the effective radius is situated in the plane of the CP whereas the maximum radius is located in the region between the two planes of the rings. The smallest radii, corresponding to the plane of the CPs, present slightly different values that vary alternately from smaller to bigger from one CP to the next all along the nanotube. This variation is due to the structure of the original crystal of the dimer used in the construction of the nanotube (Figure 3f). However, these values tend to homogenize after the MD simulation (Figure 3g). Before MD simulation, the presence of the four hydroxyl groups in the same CP (SCP_N4OH) leads to the smallest global effective radius (0.197 nm), whereas the dihydroxylated SCP_N2OH(e) and SCP_N2OH(a) have slightly bigger effective radii (0.246 and 0.266 nm, respectively) and these are closer to that of the non-derivatized pore (0.284 nm). The values for the dihydroxylated systems are maintained after MD simulation (0.254 and 0.268 nm for SCP_N2OH(e) and SCP_N2OH(a), respectively), whereas the effective radius for SCP_N4OH and the pristine SCPN increased considerably once these systems had been simulated (0.247 and 0.306 nm, respectively). Besides, whereas in the SCPN without functionalization the regions corresponding to the α - α and γ - γ interactions are indistinguishable in size, the inner hydroxylation of the channels decreases the region corresponding to the α - α interaction in all the pores with respect to the γ - γ region. This change is due to the equatorial orientation of hydroxyl groups, which are projected towards the α - α interface area (Figure 3e). This effect is much less marked after MD simulation, but it is still observed for SCP_N2OH(a).

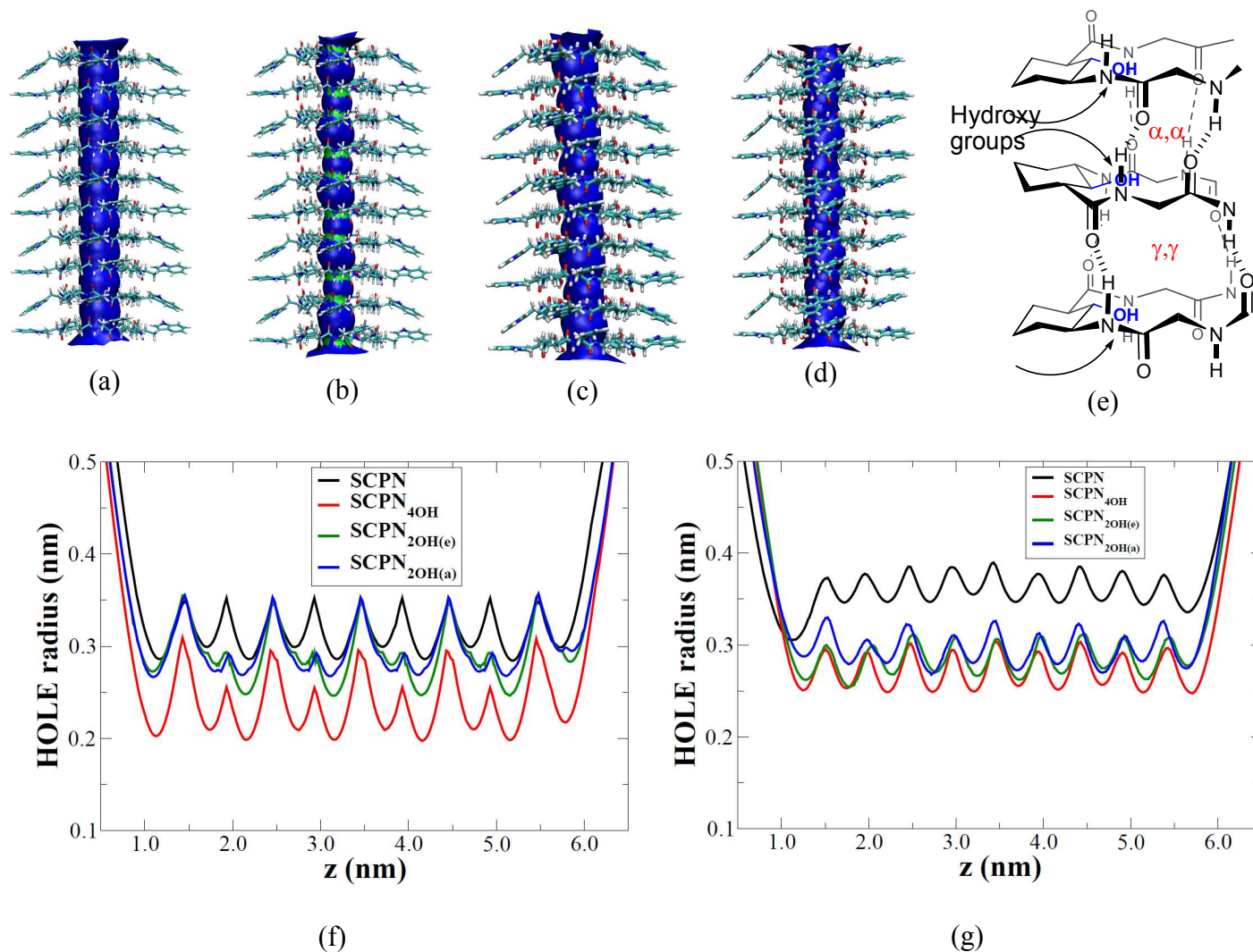
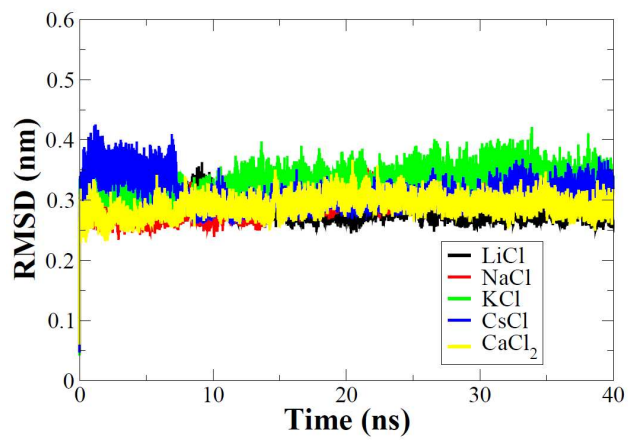


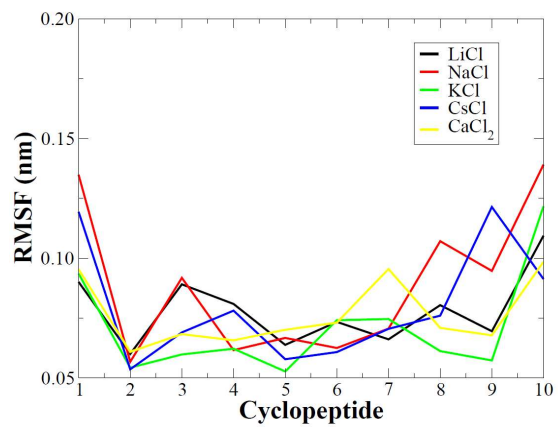
Figure 3: HOLE³⁶ radius for SCPN (a), SCPN_{4OH} (b), SCPN_{2OH(e)} (c), and SCPN_{2OH(a)} (d), and a graphical comparison between all systems along the principal axis before MD simulations (f) and averaged during the whole MD simulation (g). A detail of the equatorial position of the hydroxyl groups is shown in (e).

Both the bilayer and all fifteen simulated systems (the three derivatized nanotubes immersed in different salt solutions) were stable during the simulated time. The channel structure was well preserved, as shown by the root-mean-square deviations (RMSD) and root-mean-square fluctuations per cyclopeptide (RMSF) (Figure 4). The most flexible system is SCPN_{2OH(e)} simulated in 0.5 M LiCl, as

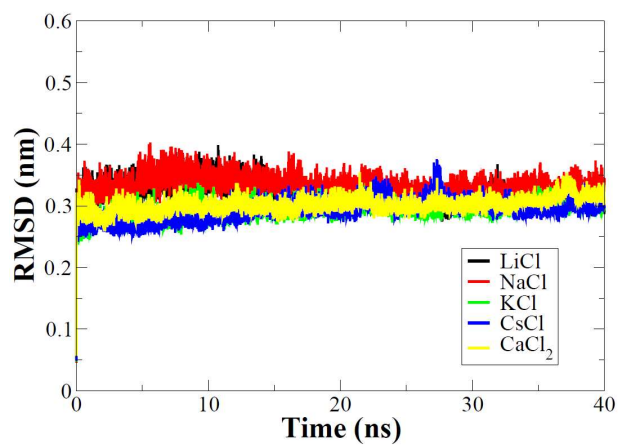
deduced from its higher RMSDs. This flexibility is induced not only by the movement of the terminal CPs, but also by a more marked fluctuation of the central units of the nanotube. Analysis of the radii of gyration (R_g) of the backbone of each CP confirms the absence of any major global or local structural distortion during the trajectories, indicating that the rings remain in a quite flat conformation (see Supplementary Figures S1–S3). However, some slight variations are observed in the range of 0.05 nm and this suggests that the CPs are quite flexible along the simulation, again mainly in the $\text{SCP}_{\text{N}_2\text{OH}}(\text{e})$ system.

SCPN_{4OH}

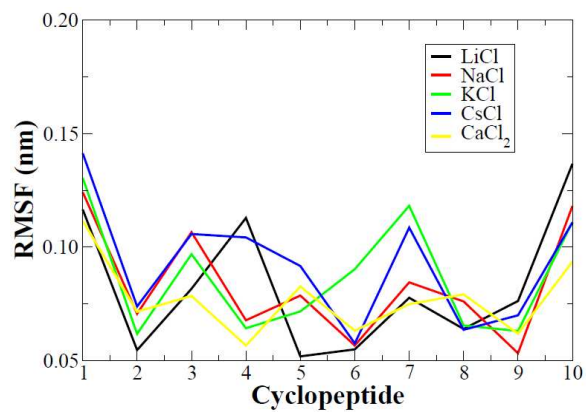
(a)



(b)

SCPN_{2OH}(a)

(c)



(d)

SCPN_{2OH}(e)

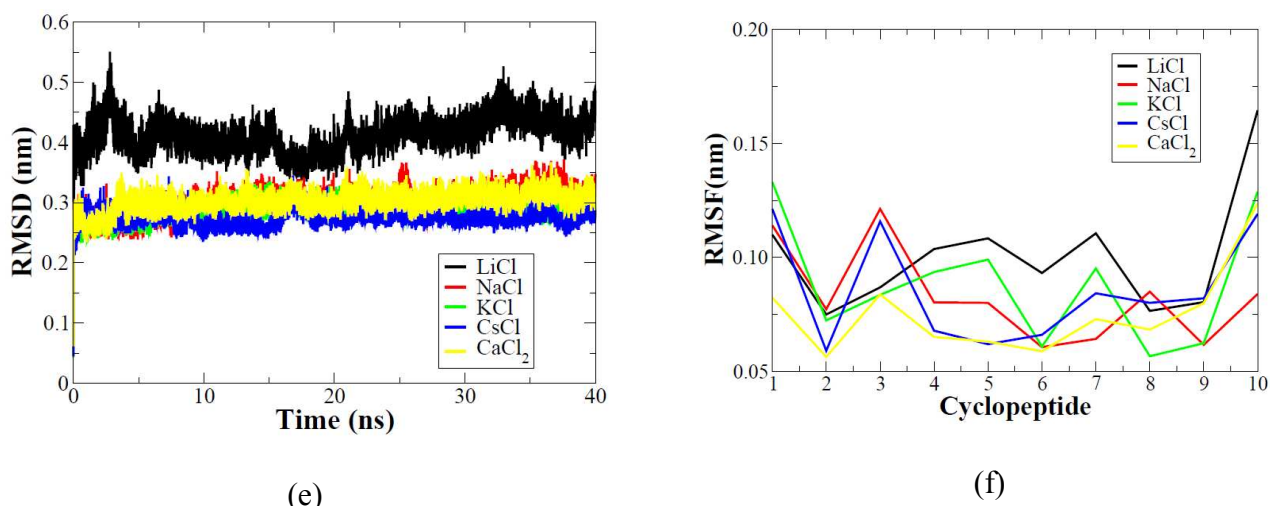
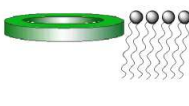
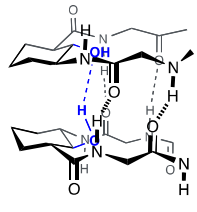
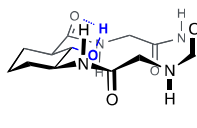


Figure 4: RMSD and RMSF for the three derivatized nanotubes **SCPN_{4OH}** (a-b) **SCPN_{2OH}(a)** (c-d) and **SCPN_{2OH}(e)** (e-f), simulated in different salt solutions for 40 ns and considering all atoms of the SCPN.

The formation of hydrogen bonds (H-bonds) between the self-assembled CPs is reduced from the theoretical 72 inter-CP H-bonds per nanotube to an average 3–6 H-bonds in **SCPN_{4OH}**, 4–5 H-bonds in **SCPN_{2OH}(a)** and 5–16 H-bonds in **SCPN_{2OH}(e)** (where the larger number corresponds to the most flexible system resulting from the simulation of the eclipsed dihydroxylated nanotube in 0.5 M LiCl) due to competition with water molecules and, to a lesser extent, lipids (Table 1). The inner functionalization with hydroxyl groups introduces a new donor group, the OH covalently linked to the cycloalkane moiety, and these, in principle, could also participate in the formation of H-bonds with the other donors/acceptors in the nanotubes. However, the hydroxyl groups seem to be too far away to form H-bonds with one another and intramolecular H-bonding between OH groups attached to a same CP or from neighboring units (OH–OH, Table 1) is practically non-existent. In spite of this situation, OH groups do participate in H-bonds with the C=O and NH groups of the CP to which they are attached and they establish an average of 1–3 H-bonds of this type and also compete with the H-bond network responsible for maintaining the channel structure (CP–OH, Table 1). The number of H-bonds between the nanotube and the aqueous solvent (CP–Water) is enhanced for **SCPN_{4OH}**, **SCPN_{2OH}(a)**, **SCPN_{2OH}(e)**

in comparison to the non-derivatized SCPN to about 51–57, 21–29 and 25–29 H-bonds, respectively,¹³ and this is mainly due to the participation of the hydroxyl groups present in the lumen of the channel.

Table 1: Mean and standard deviation of the number of H-bonds between different components of the simulated systems in different salt solutions for 40 ns.

		CP-CP 	CP-Water 	CP-DOPC 	OH-OH 	CP-OH 
SCP_N4OH	LiCl	69 ± 3	125 ± 7	2 ± 1	-	2 ± 1
	NaCl	69 ± 3	123 ± 8	2 ± 2	-	2 ± 2
	KCl	66 ± 3	120 ± 8	3 ± 2	-	3 ± 2
	CsCl	67 ± 3	120 ± 7	3 ± 2	-	3 ± 2
	CaCl₂	67 ± 3	126 ± 9	2 ± 2	-	3 ± 2
SCP_N2OH(a)	LiCl	67 ± 2	97 ± 7	1 ± 1	-	1 ± 1
	NaCl	67 ± 2	97 ± 7	2 ± 1	-	1 ± 1
	KCl	68 ± 2	89 ± 6	3 ± 1	-	1 ± 1
	CsCl	68 ± 2	95 ± 7	2 ± 1	-	1 ± 1
	CaCl₂	67 ± 3	100 ± 8	2 ± 1	-	2 ± 1
SCP_N2OH(e)	LiCl	56 ± 3	106 ± 7	3 ± 1	-	1 ± 1
	NaCl	66 ± 3	97 ± 7	2 ± 1	-	1 ± 1
	KCl	66 ± 3	93 ± 7	3 ± 1	-	1 ± 1
	CsCl	67 ± 3	98 ± 7	3 ± 1	-	1 ± 1
	CaCl₂	67 ± 3	99 ± 8	2 ± 1	-	1 ± 1

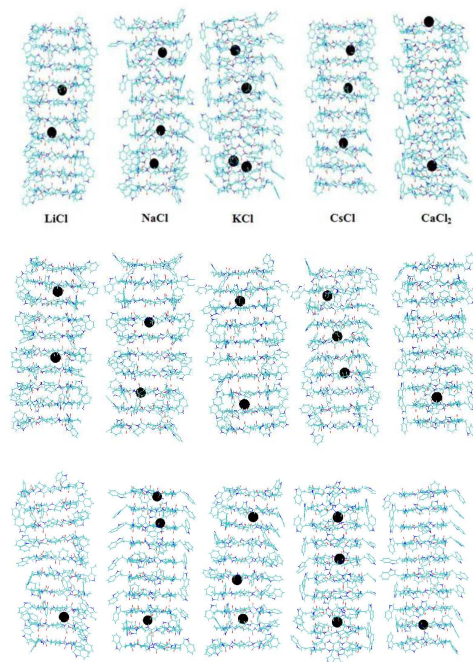
The entrance of water molecules and cations is observed very promptly (see Supplementary Figure S4) during the first nanoseconds for all the systems and all the salt solutions studied. As a result, we are confident that a 40 ns simulation is sufficient to provide an equilibrium, or close to equilibrium, picture of ions within the nanopore. The number of ions present inside each of the SCPNs was analyzed over

the course of the simulations (Table 2). As in the case of *D,L*- α -SCPNS,^{20d} under these conditions Cl⁻ anions sometimes remained at the nanotube entrance and they never really penetrated into the channel. This strong selectivity for cations is attributed to the negatively charged carbonyl oxygens inside the channel and it is enhanced by the presence of the OH groups in the modified channels.³⁷ The standard deviation for water molecules inside SCPN_{4OH} is higher than for the systems bearing only two hydroxyl groups in the CPs, suggesting a higher level of water renovation for the tetrahydroxylated channel.

The three derivatized nanotubes simulated in 0.5 M LiCl and 0.5 M CaCl₂ admit, on average, ca. 2 and 1 cations, respectively, i.e., the same number of cations found inside the non-derivatized channels.¹³ The introduction of the OH groups allows the entrance of an extra Cs⁺ cation in all the derivatized pores and an extra K⁺ cation in SCPN_{4OH} and SCPN_{2OH}(e). The entrance of Na⁺ ions is slightly preferred inside SCPN_{4OH} than in the dihydroxylated channels.

Table 2: Mean and standard deviation of the number of ions and water molecules inside the nanotubes, simulated for different salt solutions for 40 ns.

		Cations	Anions	Water
SCP _N _{4OH}	LiCl	2 ± 0	-	84 ± 15
	NaCl	3 ± 1	-	84 ± 16
	KCl	3 ± 1	-	85 ± 18
	CsCl	3 ± 1	-	82 ± 15
	CaCl ₂	1 ± 0	-	85 ± 18
SCP _N _{2OH} (a)	LiCl	2 ± 1	-	85 ± 6
	NaCl	2 ± 0	-	86 ± 6
	KCl	2 ± 0	-	82 ± 5
	CsCl	3 ± 1	-	79 ± 7
	CaCl ₂	1 ± 0	-	85 ± 7
SCP _N _{2OH} (e)	LiCl	2 ± 0	-	88 ± 7
	NaCl	2 ± 1	-	86 ± 7
	KCl	3 ± 1	-	84 ± 7
	CsCl	3 ± 1	-	82 ± 6
	CaCl ₂	1 ± 0	-	86 ± 8



Besides the number of ions inside the channels it is possible to monitor their positions in the lumen of the corresponding nanotubes for each frame of the trajectory (Figure 5). It is noticeable that, whereas transport along the channel was not observed in the equilibrium simulations carried out with the non-derivatized nanotube for any of the cations studied, the introduction of 4 hydroxyl groups and even of only two of them in the lumen of the nanotubes led to the net flux of one Cs^+ cation in the first 20 ns of the simulation. To our knowledge, this is the first time that the passage of ions has been detected through a transmembrane nanotube without the need to apply a transmembrane voltage or concentration gradient. However, since the systems are simulated under equilibrium conditions, one would expect to observe inverse diffusion (in the opposite direction) if simulation times were sufficiently long. With the exception of Cs^+ , it should be pointed out that once the ions enter the nanotube, they remain inside for the whole simulation time. Whereas Li^+ cations penetrate deeper into the lumen of $\text{SCP}_{\text{N}4\text{OH}}$ than in the rest of the studied channels, the Ca^{2+} ion remains nearer to the edges of the hydroxylated pores than it did in the pristine channel,¹³ presumably because the stronger interaction with the OH groups makes its passage through the nanopore more difficult. Most of the ions inside the hydroxylated channels spend more time in the regions between the planes of CPs that interact through an α - α interaction in spite of their smaller initial effective radius compared to the γ - γ area. This observation suggests that these regions act as brakes against the advance of the ions along the pore.

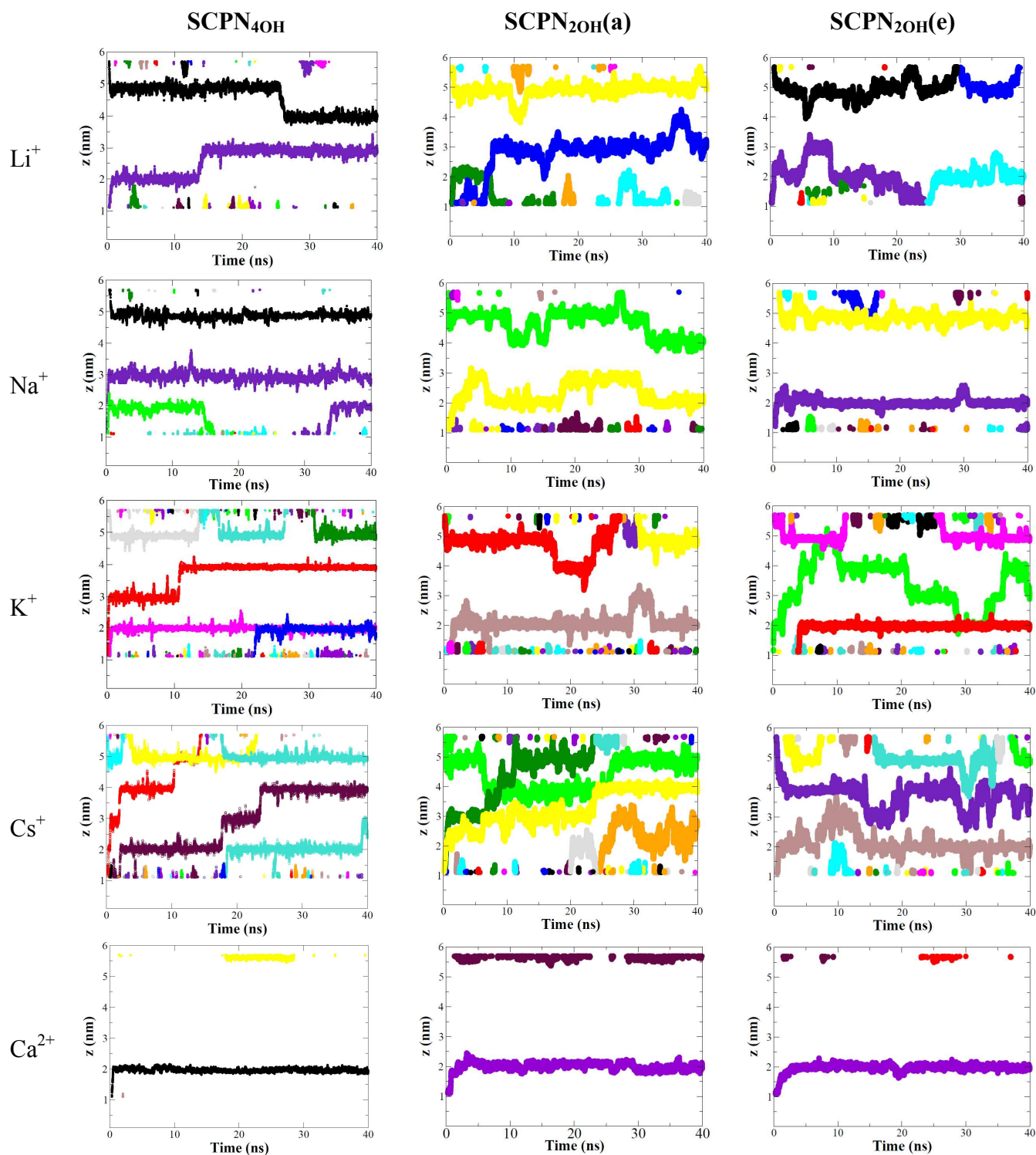


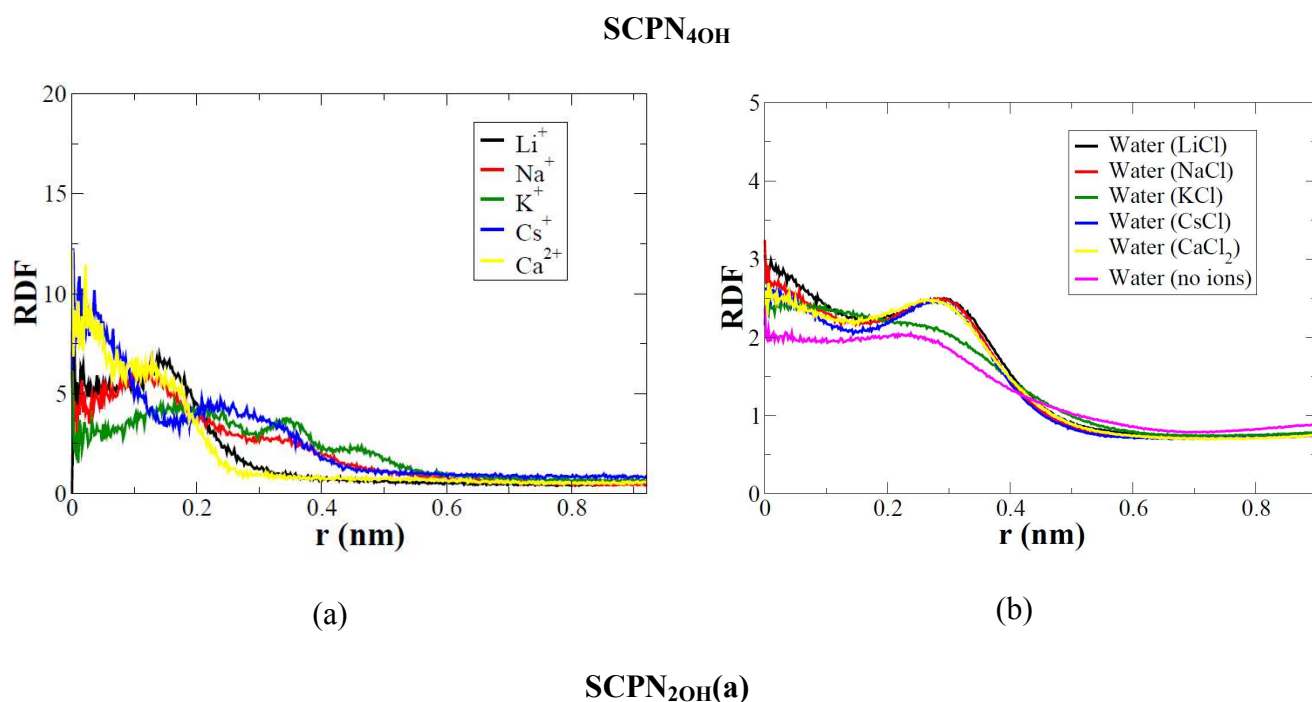
Figure 5: z-coordinate for each of the cations inside the simulated peptide nanotubes along the 40 ns trajectory. The nanotube z-region is comprehended between the region ~ 1 -6 nm. Each color corresponds to a different ion.

In most of the simulations there is a short co-existence of two ions inside the channels in regions that are very close in space, but this situation is very short-lived and when two cations are close one of them rapidly displaces the other one. However, when **SCPN_{4OH}** was simulated in 0.5 M KCl two K⁺ cations coexisted very close to each other (at a distance ~0.4–0.7 nm) along half of the trajectory (see Supplementary Figure S5). The proximity of the two cations was maintained in the trajectory for about a further 30 ns (see Supplementary Figure S6a). Nevertheless, this situation was not reproducible on repeating the same simulation several times, suggesting that this is not a general phenomenon (see Supplementary Figure S6b).

Radial distribution functions (RDF) of the cations and water inside the nanotube on the xy axes describe how its density varies with respect to the center of the nanotube, thus giving an average of how they are radially packed (Figure 6). Ca²⁺ and Cs⁺ cations tend to accumulate at the center of the three studied channels, whereas for the other cations the distribution is more spread out. The behaviors of Li⁺ and Na⁺ cations are very similar in **SCPN_{4OH}** and **SCPN_{2OH(a)}**. In **SCPN_{2OH(e)}**, Li⁺ ions mainly tend to populate the center, whereas Na⁺ also moves close to the walls of the channel. In the case of K⁺, in spite of having less space in the cavity in the presence of the four hydroxyl groups, there is a populated position further away from the center than in the dihydroxylated channels.

As in *D,L-α*-SCPNS^{20j} and nonpolar nanoenvironments such as carbon nanotubes,³⁸ water inside the simulated *α,γ*-SCPNS was highly structured. Despite the presence of ions inside the channels, there is a significant degree of structuring of the water within the nanopores, as seen previously.¹³ The water presents a maximum at about 0.3 nm in almost all the systems studied, although in **SCPN_{4OH}** it tends to accumulate at the center of the nanotube (Figure 6). The internal water populates the two different regions that exist in the channel along the nanotube axis (see Supplementary Figure S7), i.e. those corresponding to the regions between the planes of the CPs (more populated) and those corresponding to the regions of the plane of the CP (less populated). However, while in the pristine *α,γ*-SCPNS water tends to follow a –4–5–4–5– pattern, where 4 is the number of water molecules located in the plane of

the CP and 5 those between the planes of the CPs,¹³ the introduction of four or two hydroxyl groups in the lumen of the channel causes a slight change in this disposition to a -3-5-3-5- pattern, i.e., decreasing the total number of water molecules inside the channel (to about 5 water molecules). This change is probably due to the decrease of the inner volume of the nanopore caused by the presence of the hydroxyl groups (see Supplementary Figure S8).



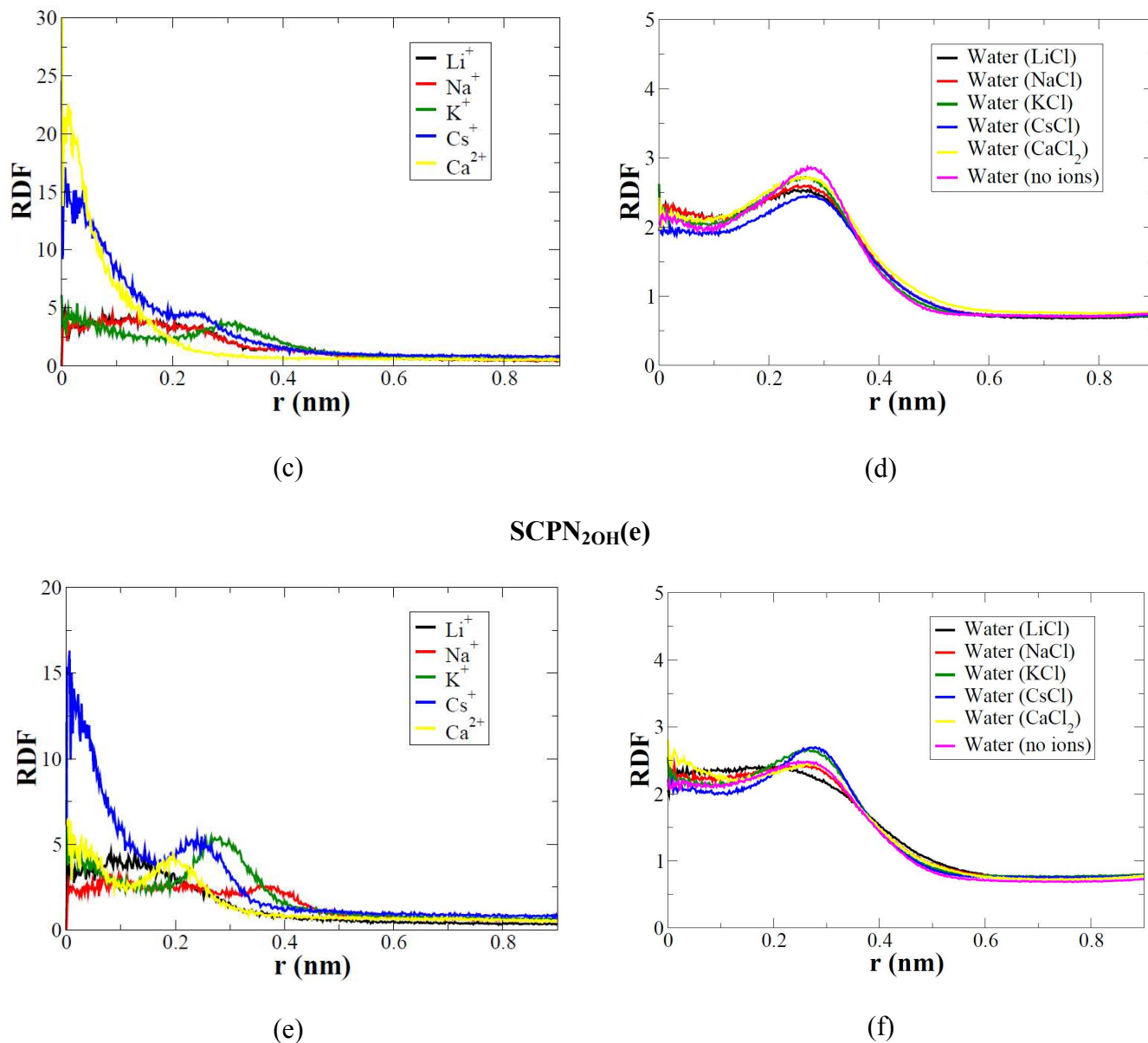


Figure 6: Radial Distribution Function (RDF) in the xy direction for the cations and water along 40 ns of simulations of the peptide nanotubes at different salt solutions with respect to the center of the nanotube, for the three derivatized nanotubes $\text{SCP}_{\text{N}4\text{OH}}$ (a-b) $\text{SCP}_{\text{N}2\text{OH}}$ (a) (c-d) and $\text{SCP}_{\text{N}2\text{OH}}$ (e) (e-f).

Analysis of the diffusion coefficients of ions along the nanopore axis shows that the ion diffusion coefficients are lower than those observed in the bulk, as was also found for simulations of ions in smooth cylindrical channels (see supplemental Table S1).³⁹ It should be noted, however, that the large

standard deviations associated with the diffusion coefficients suggest that longer simulation times would be needed for a confident quantitative comparison of this factor.

The radius for the first coordination sphere of each cation inside the derivatized nanotubes can be envisaged from the cation-O (water) radial distribution profiles (see Figure 7). The profiles are reasonably consistent with the values found previously for these types of cations in other theoretical calculations⁴⁰ and also in the pristine peptide nanotubes (Figure 7a).¹³ The peak corresponding to the position of the second coordination sphere is also very similar for the functionalized and non-functionalized nanopores. No oxygen from the hydroxyl group of CP participates directly in the first coordination sphere of Li^+ and Ca^{2+} , whereas for Na^+ , K^+ and Cs^+ a small presence of oxygens (1–2) from the C=O and OH groups is detected, a situation that is also reflected in the increase of the total coordination number for these ions (Table 4 and Supplementary Figures S9 and S10). The number of oxygens coordinated to the cations inside the three derivatized nanotubes is very similar, with values around 4, 5, 8, 8 and 9 for Li^+ , Na^+ , K^+ , Cs^+ and Ca^{2+} , respectively (Table 4). The main differences with respect to the pristine SCPNs are found for Na^+ , K^+ and Cs^+ , i.e., the ions with which oxygens from C=O and OH groups participate in the first coordination sphere. The balance between size and charge for Li^+ and Ca^{2+} results in a stronger interaction between these cations and their water coordination spheres, while for Na^+ , K^+ and Cs^+ oxygens from other coordinating groups, such as the C=O and OH groups of the CP, can also participate in the first coordination shell.

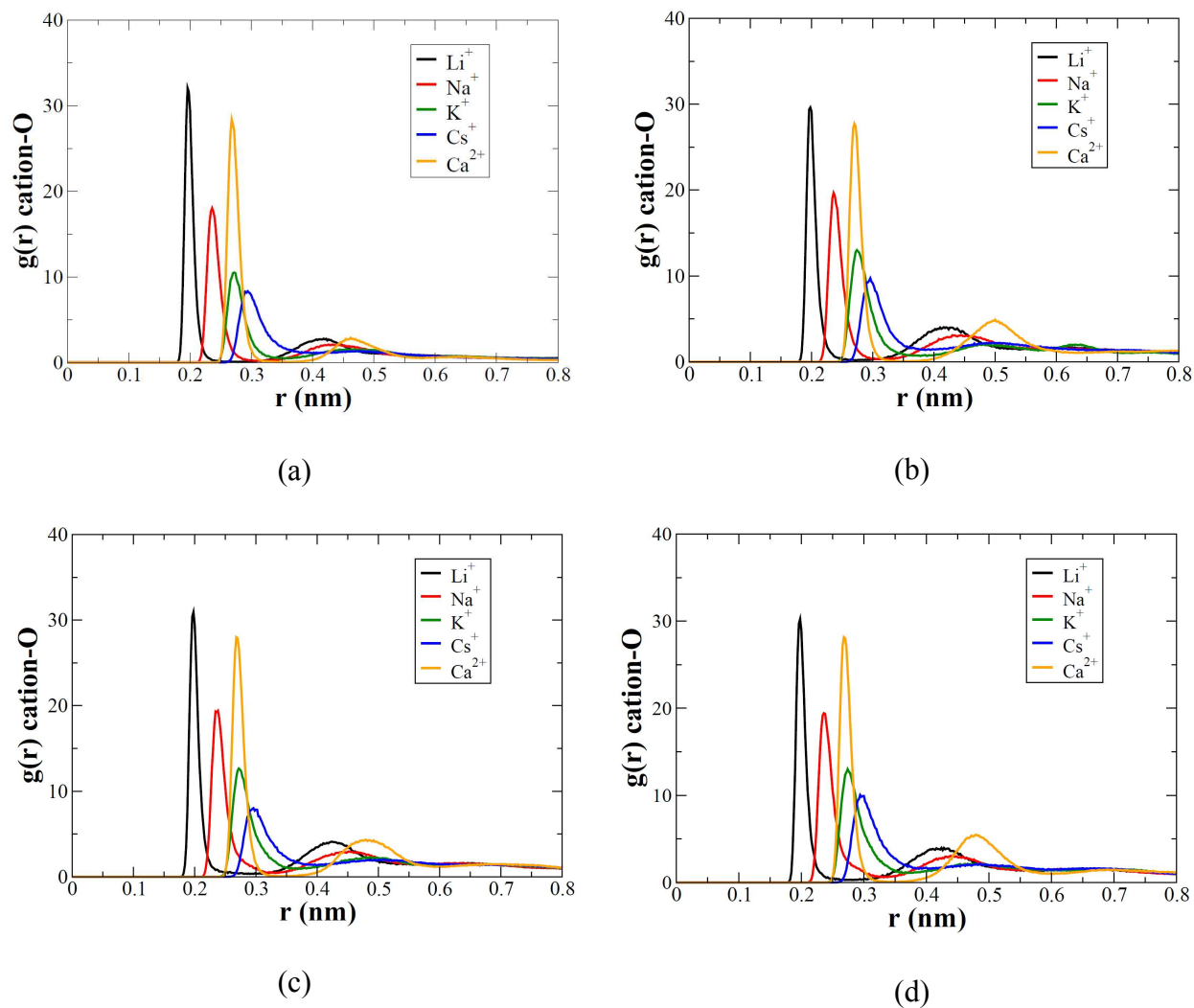


Figure 7: Radial distribution of the cation-O distance inside the nanotube [$g_{\text{ion-oxygen}}(\mathbf{r})$] for the non-functionalized SCPN (a), SCPN_{4OH} (b), SCPN_{2OH}(a) (c), SCPN_{2OH}(e) (d) considering the contribution of all the oxygens (water + C=O + OH).

Table 4: Mean and standard deviation of the number of oxygens coordinated to the cations inside the nanotubes in the first coordination sphere. Oxygen atoms from different sources (water, C=O and OH).

		O (H₂O + C=O + OH)	O (C=O)	O (OH)
SCPN_{4OH}	LiCl	4 ± 0	0 ± 0	0 ± 0
	NaCl	5 ± 1	0 ± 0	0 ± 1
	KCl	8 ± 2	1 ± 1	2 ± 1
	CsCl	8 ± 2	1 ± 1	1 ± 1
	CaCl₂	9 ± 1	0 ± 0	0 ± 0
SCPN_{2OH(a)}	LiCl	4 ± 0	0 ± 0	0 ± 0
	NaCl	5 ± 1	0 ± 1	0 ± 1
	KCl	8 ± 2	1 ± 1	1 ± 1
	CsCl	8 ± 2	1 ± 1	1 ± 1
	CaCl₂	9 ± 1	0 ± 0	0 ± 0
SCPN_{2OH(e)}	LiCl	4 ± 0	0 ± 0	0 ± 0
	NaCl	5 ± 1	0 ± 1	1 ± 1
	KCl	9 ± 2	1 ± 1	2 ± 1
	CsCl	9 ± 2	0 ± 1	1 ± 1
	CaCl₂	9 ± 1	0 ± 0	0 ± 0

The lack of replacement of any water in the first coordination spheres of Li⁺ and Ca²⁺ suggests that with these cations the first shell remains intact during the transport process across the channel. This behavior is translated into much more marked (and more favorable) differences between the interaction energy of the cation with the surrounding water than with the nanotube for Li⁺ and Ca²⁺ (see Supplemental Figure S11). The replacement of water in the coordination shell of Na⁺ with the nanotube yields a less favorable ion-water interaction whereas the lack of replacement of water in the hydration shell of Ca²⁺ leads to a more propitious ion-water interaction all along the simulated channels. The retention of the first hydration sphere in Ca²⁺ has been also observed experimentally, for example in Ca_vAb, a modified channel for Ca²⁺ conduction from the biological sodium channel Na_vAb.⁴¹ In the crystal structure of the mutated biological channel Ca²⁺ is surrounded by a box of four carboxylate oxygen atoms from D177 above and four backbone carbonyl oxygen atoms from L176 below, with oxygen–Ca²⁺ distances of 4.5 and 4.2 Å, respectively (Figure 8a). Most of the distances from the hydroxyl groups to Ca²⁺ in SCPN_{4OH} are also in this range, with the oxygens located in two planes in a

similar disposition to that found in Ca_vAb (Figure 8b). It can be thus envisaged that derivatized α,γ -SCPNs could be successfully used as biomimetic of channels when properly inner-functionalized.

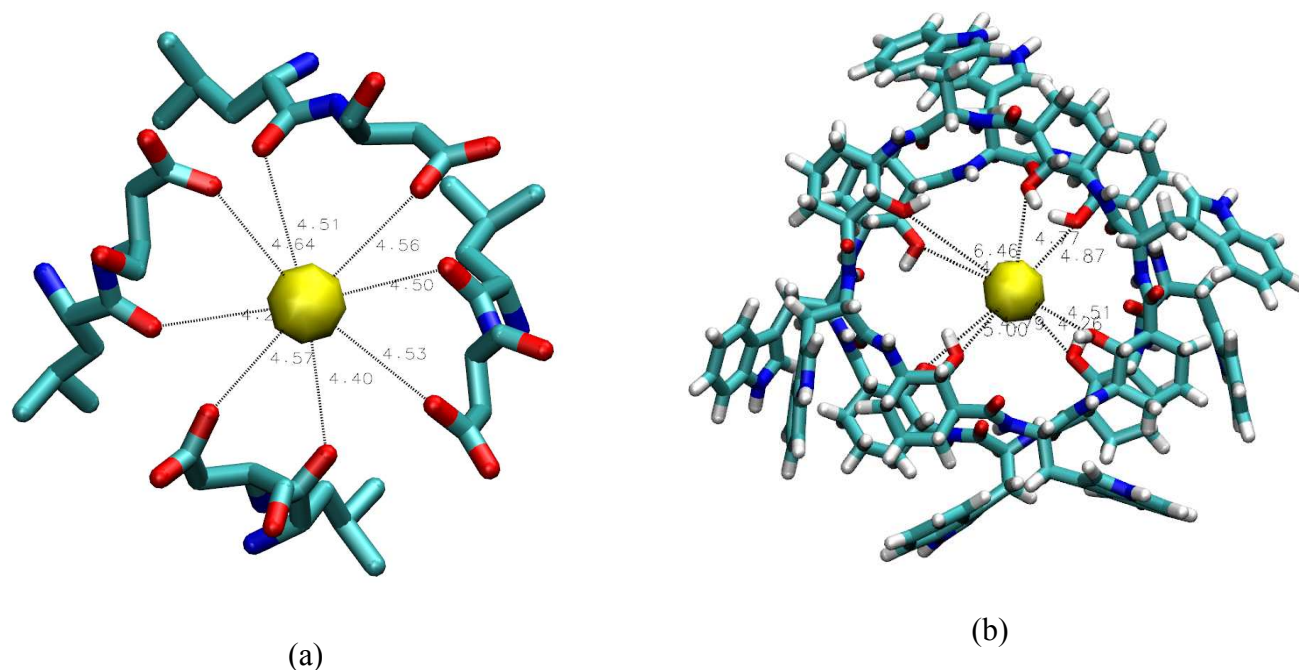


Figure 8: Detail of the coordination of Ca^{2+} with the oxygens from the crystal of Ca_vAb (a) and the CPs in $\text{SCP}_{40\text{H}}$.

The thermodynamics of ion movement in the nanotubes were explored by calculating the single-ion potential of mean force (PMF), i.e., the free energy of the ion as a function of its z coordinate (the coordinate running parallel to the channel axis) when other ions are excluded from the channel (Figure 9 and Supplementary Figure S12). In spite of the known difficulties of the actual ion parameters in explaining the energetics of permeation of monovalent cations, and binding and blocking of divalent cations, it has been also demonstrated that nonpolarizable force fields can account for the binding configurations of monovalent and divalent cations.⁴² The parameters used for the ions are implemented in AMBER, and have been used to justify and reproduce experimental results.¹³ Furthermore, another validation of these parameters has been carried out comparing the interaction energy values obtained in similar structures for different ions using B3LYP/6-31G(d) (see Supplementary Table S2), obtaining a

good qualitative agreement between the quantum calculations and the parameters used in the present work.

Inside the tube, the repeating structural motif creates a series of energy barriers and troughs descending to a central global minimum; the fact that this series is much less well-defined than for D,L- α -SCPNS is probably attributable, at least in part, to the larger size of the α,γ -SCPNS and also to the absence of restrictions in the CPs in the calculation of PMFs. It is precisely the absence of restrictions in the nanotube that makes convergence difficult for these systems and longer simulation times (unaffordable for the present study) would be required to make a quantitative comparison of the values obtained in the PMF study. A qualitative analysis of the energy profiles shows that the central global minimum is deeper for Ca^{2+} , although a certain degree of selectivity of Ca^{2+} over alkali metal ions is lost with the hydroxylation of the pristine nanotube (Figure 9). As it has been deduced from the equilibrium MD simulations, channels can accommodate more than one alkaline cation, whereas only one single Ca^{2+} was found inside the pore. We are aware that conductance studies rely on kinetics of transport and therefore multiple binding sites are a factor to worry about, and the results should be interpreted with caution.⁴³ However, the actual study only aims to see the effect of hydroxyl groups on the transport of some alkaline cations compared to Ca^{2+} , and even the 1D PMFs suggest that the inner functionalization does not affect the selectivity of the cations to a great extent, with only small differences with respect to the non-derivatized SCPNS.

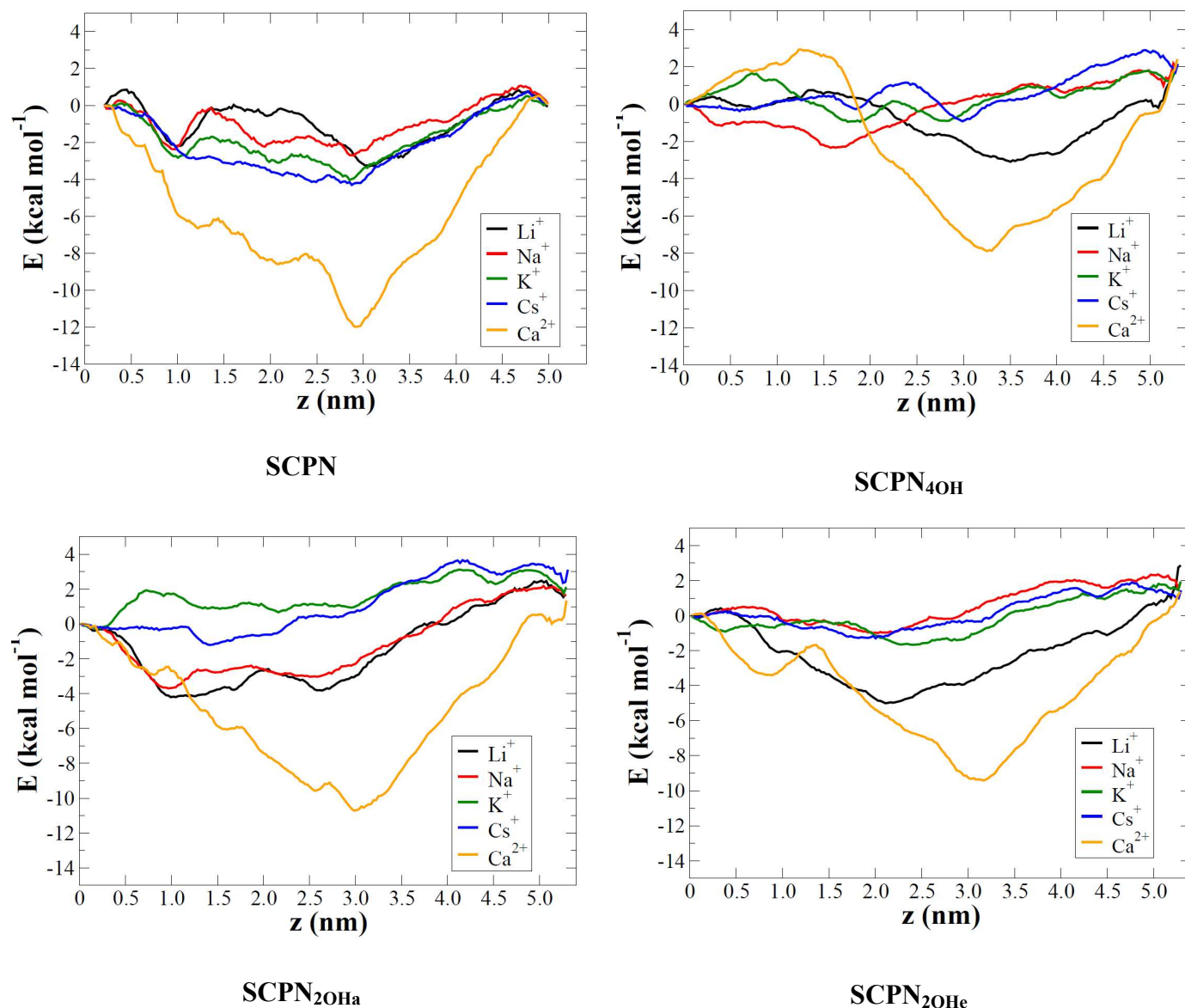


Figure 9: Potentials of Mean Force (PMF) for single ions as a function of position along the z-axis of each one of the studied pores.

Although the incorporation of the hydroxyl groups at the lumen of the channels did not provide higher selectivity in the transport of ions across the membrane, the chemical versatility of this moiety would offer the opportunity to further incorporate other chemical modifications of the inner of the nanotubes, tuning the SCPN properties, something impossible in other nanotube constructions.⁴³ Such modifications would open the door to a variety of application in sensing, signaling and catalysis.

For example, protection/deprotection of hydroxyl groups is one of the most common reactions in organic chemistry. To avoid interference by hydroxyl groups, it is often necessary to mask them by conversion to less reactive functions, such as ethers, esters, or acetals. These processes are generally reversely and both transformations (protection and deprotection) are carried out under very mild conditions, allowing to modulated control of the moiety supported by the oxygen of the alcohol. In this sense, decorated CPs with hydroxyl groups at their inner cavities would permit to adjust both size and functionality of the groups projected into the lumen of the pores just regulating the reagents needed for a typical protection/deprotection of alcohols in a chemical reaction. For example, β -methoxylation of all γ -residues of the channel forming cyclic peptide (**CP_{4OMe}**) could transform active ion transporter channels into transport blocked structures. This strategy enables a controlled method for the activation/inactivation of the nanopore. Trying to explore this concept, MD simulations on the methoxylated channel (**SCP_{N4OMe}**) inserted into a DOPC lipid bilayer were carried out under different salt solutions (NaCl and CaCl₂ 0.5 M) (Figure 10). The cyclic α,γ -octapeptides modified at the C2 position resulted in a stable cylindrical structure (See Supplemental Figure S13), with a HOLE³⁶ radius of 0.96 nm, \sim 50% smaller than the tetrahydroxy-functionalized SCPN (**SCP_{N4OH}**). **SCP_{N4OMe}** maintained the tubular shape in the membrane while also created an almost dry confinement inside the pore, free of ions, thus confirming the transport inhibition properties (Figure 10). The selection of appropriate chemical labile groups for the inner hydroxyl moieties could make possible to achieve a reversible control based on the environmental conditions, suggesting potential application in novel controlled drug release systems.

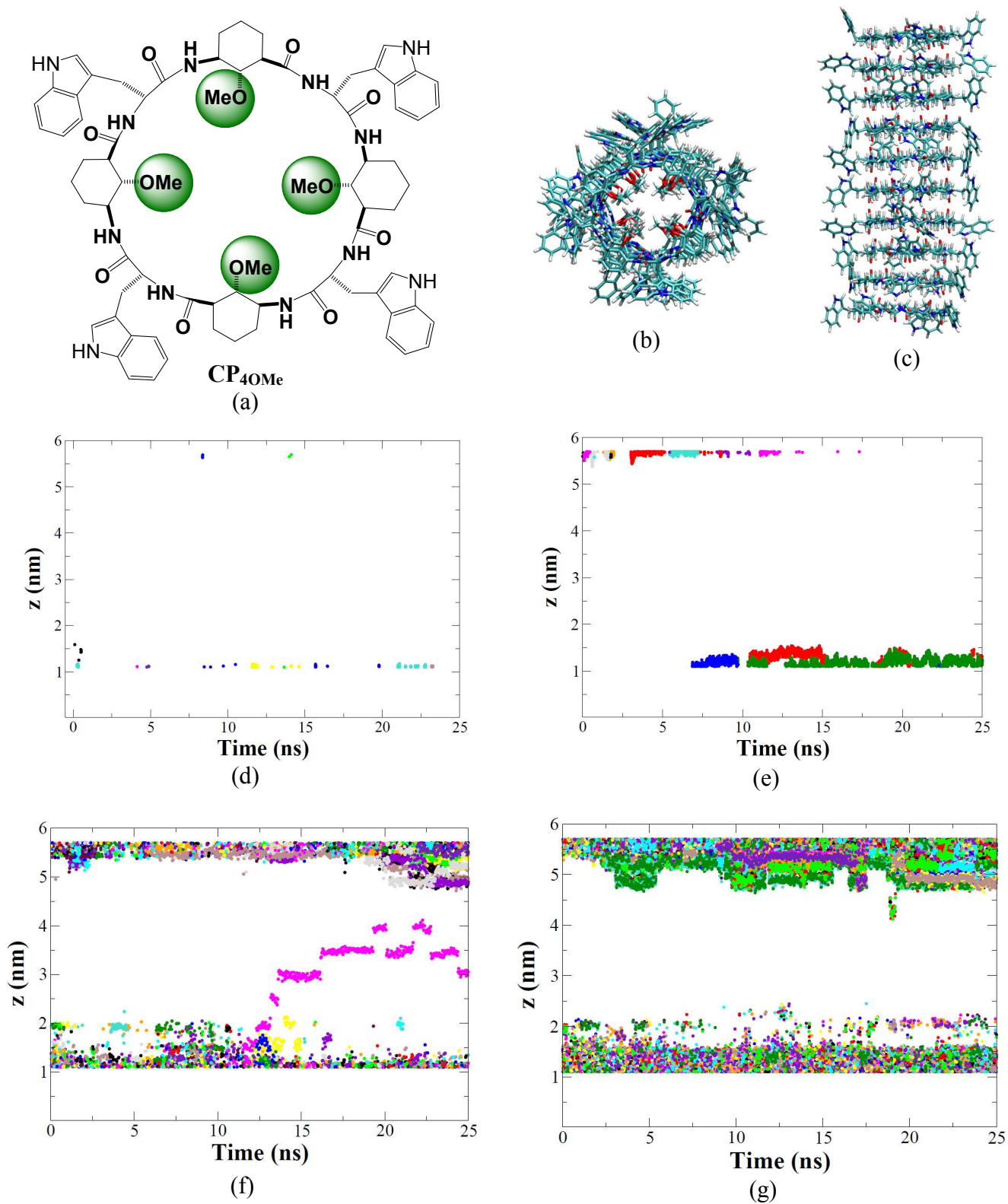


Figure 10: (a) Hydroxymethylated CPs composing SCPN_{40Me}. (b-c) Top and lateral views of a snapshot (25 ns) from the simulation of SCPN_{40Me} in CaCl₂. (d-e) Z-coordinate for each of the cations (Na⁺ or

Ca^{2+}) and (f-g) Z-coordinate for each water oxygen inside the simulated SCPN_{40Me} along 25 ns in NaCl or CaCl₂, respectively. Each color corresponds to a different ion or water molecule.

Conclusions

In this work we have used the great potential of MD simulations to study a supramolecular system of nanometric dimensions, namely peptide nanotubes formed by the combination of CPs with alternating α - and γ -amino acids from *D*- α -amino acids and γ -Aca, respectively. Such nanostructures have certain advantages over other known types of nanotubes, perhaps the most important being the possibility of inner functionalization. Taking advantage of this functionality, three nanotubes were designed in which the γ -amino acids provide hydroxyl groups that are oriented inwards into the internal cavity. In all cases the presence of hydroxyl groups increases the hydrophilic character of the cavities in a controlled manner. The influence that these functional groups have on the ion transport through a DOPC lipid bilayer, using different salt solutions (0.5 M LiCl, NaCl, KCl, CsCl and CaCl₂, respectively) was investigated at atomic resolution.

The results obtained suggest that these artificial derivatized channels are stable in the lipid environment, despite competition between H-bonds established with water, lipids and the hydroxyl groups and those necessary to maintain the network of H-bonds along the entire channel. The introduction of hydroxyl groups into the cavity of SPCNs maintains the channel selectivity to cations and the entry of Cl⁻ anions was not observed in any of the simulations studied. The presence of four hydroxyl groups in the lumen of the CPs allows the introduction of one extra Na⁺, K⁺ and Cs⁺ ion (with respect to the non-functionalized SCPN), whereas the channels composed of dihydroxylated CPs only incorporate an extra Cs⁺ ion (and an extra K⁺ ion when the orientations of the CPs are alternate). The functionalization of the lumen also affects to the disposition of the water inside the pore. Within the pristine SPCNs the internal water followed a 4-5-4-5 profile, where 4 is the number of molecules located in the plane of the corresponding CP and 5 the number of water molecules between the planes of the CPs. However, the

introduction of the hydroxyl groups led to a slight change in this distribution towards a 3-5-3-5 profile, with a slight decrease in the number of water molecules found within the channel (around five molecules). This change is probably due to the lower volume of the interior of the channel caused by the presence of hydroxyl groups.

The balance between size and charge for Li^+ and Ca^{2+} results in a stronger interaction between these cations and their water coordination spheres, maintaining them along all the simulation. Taking into account that retention of the first hydration sphere in Ca^{2+} has also been observed experimentally in some biological channels together with the fact that the distances from the hydroxyl groups to Ca^{2+} in the hydroxylated nanotubes are in the range and similar disposition than in the filters of some biological channels, it can be easily envisaged that inner-functionalized nanotubes based on α,γ -CPs offer a promising future for their use as biomimetic channels, when properly inner functionalized. Potential of mean force (PMF) calculations for the three hydroxylated nanotubes confirm that the inner functionalization does not affect the selectivity to the cations to a great extent, with only small differences observed in comparison to the non-derivatized SCPNs, and suggest that bigger and/or charged functional groups are needed to affect the stripping of their hydration shell. In spite of not providing higher selectivity among ions, an inner cavity decorated with hydroxyl groups would enable to other chemical modifications inside the nanotubes, potentially leading to very attractive applications, such as the reversible control of the transport in the channel. MD simulations on a β -methoxylated channel inserted into a lipid membrane resulted into an ion transport blocked nanotube. The hydroxymethylated pores maintained the tubular shape at the same time that completely stopped the transport of ions and even most of water molecules across the membrane, enabling a controlled method for the activation / inactivation of the nanopore. Our results predict a great potential for biomimetic pores based on internally functionalized self-assembling α,γ -peptide nanotubes and encourage chemists to strive for the development of synthetic methodologies that would allow in-vitro studies with this

systems, at the same time that confirm the power of MD simulations to assist in the design of new artificial channels that mimic Nature more accurately.

Acknowledgments

We are grateful for funding from the Spanish Ministry of Science and Innovation MICINN and the ERDF (CTQ2010-15725, CTQ2013-43264-R) and the Xunta de Galicia and the ERDF (GPC2013-039 and EM 2012/117). We also thank the ORFEO-CINCA network and to the COST CM1306 European Action. All calculations were carried out at the Barcelona Supercomputer Center (BSC-RES) and on the Centro de Supercomputación de Galicia (CESGA).

Electronic Supplementary Information (ESI) available

Figures S1-S13 and Tables S1-S2.

Bibliographic references & notes

1. B. Hille. *Ion channels of Excitable Membranes*, 3rd ed.; Sinauer: Sunderland, MA, 2001.
2. (a) A. L. Sisson, M. R. Shah, S. Bhosale and S. Matile, *Chem. Soc. Rev.*, 2006, **35**, 1269. (b) J. K. W. Chui and T. M. Fyles, *Chem. Soc. Rev.*, 2011, **41**, 148. (c) T. M. Fyles, *Chem. Soc. Rev.*, 2007, **36**, 335. (d) S. Matile, A. Vargas Jentsch, J. Montenegro and A. Fin, *Chem. Soc. Rev.*, 2011, **40**, 2453. (e) J. Montenegro, M. R. Ghadiri and J. R. Granja, *Acc. Chem. Res.*, 2013, **46**, 2955. (f) S. W. Kowalczyk, T. R. Blosser and C. Dekker, *Trends Biotechnol.*, 2011, **29**, 607.
3. (a) Z. S. Siwy and S. Howorka, *Chem. Soc. Rev.*, 2010, **39**, 1115. (b) X. Hou, W. Guo and L. Jiang, *Chem. Soc. Rev.*, 2011, **40**, 2385.
4. (a) J. H. Fuhrhop, U. Liman and V. A. Koesling, *J. Am. Chem. Soc.*, 1988, **110**, 6840. (b) J. Lear, Z. Wasserman and W. F. Degrado, *Science*, 1988, **240**, 1177. (c) M. Mutter, G. Tuchscherer, C. Miller, K.-H. Altmann, R. Carey, D. Wyss, A. Labhardt, and J. Rivier, *J. Am. Chem. Soc.*, 1992, **114**, 1463. (d) Y. Kobuke, K. Ueda and M. Sokabe, *J. Am. Chem. Soc.*, 1992, **114**, 7618. (e) A. Grove, M. Mutter, J. Rivier and M. Montal, *J. Am. Chem. Soc.*, 1993, **115**, 5919. (f) S. Lee, M. Ellerby, T. Kiyota and G. Sugihara, *Controlled Drug Delivery*, 2000, **14**, 139. (g) B. Baumeister, N. Sakai and S. Matile, *Angew. Chem. Int. Ed. Engl.*, 2000, **39**, 1955. (h) C. G. Espínola, R. Pérez and J. D. A. Martín, *Org. Lett.*, 2000, **2**, 3161. (i) T. M. Fyles, *Acc. Chem. Res.*, 2013, **46**, 2847. (j) S. Futaki, D. Noshiro, T. Kiwada and K. Asami, *Acc. Chem. Res.*, 2013, **46**, 2924.
5. (a) M. Pregel, L. Jullien, J. Canceill, L. Lacombe and J. M. Lehn, *J. Chem. Soc. Perkin Trans.*, 1995, **2**, 417. (b) I. Elidrisi, S. Negin, P. V. Bhatt, T. Govender, H. G. Kruger, G. W. Gokel and G. E. M. Maguire, *Org. Biomol. Chem.*, 2011, **9**, 4498. (c) Y. Tanaka, Y. Kobuke and M. Sokabe, *Angew. Chem. Int. Ed. Engl.*, 1995, **34**, 693. (d) T. M. Fyles, D. Look and X. A. Zhou,

- J. Am. Chem. Soc.*, 1998, **120**, 2997. (e) Z. Qi, M. Sokabe, F. Donowaki and H. Ishida, *Biophys. J.*, 1999, **76**, 631. (f) N. Yoshino, A. Satake and Y. Kobuke, *Angew. Chem. Int. Ed. Engl.*, 2001, **40**, 457. (g) L. Mutihac, *Anal. Lett.*, 2010, **43**, 1355.
6. (a) S. J. Kennedy, R. W. Roeske, A. R. Freeman, A. M. Watanabe and H. R. Besch, *Science*, 1977, **196**, 1341. (b) D. Bali, L. King and S. Kim, *Australian J. Chem.*, 2003, **56**, 293. (c) U. Koert, L. Al-Momani and J. R. Pfeifer, *Synthesis*, 2004, **8**, 1129. (d) N. Sakai and S. Matile, *Langmuir*, 2013, **29**, 9031.
7. (a) M. F. M. Roks and R. J. M. Nolte, *Macromolecules*, 1992, **25**, 5398. (b) E. Abel, E. S. Meadows, I. Suzuki, T. Jin and G. W. Gokel, *Chem. Commun.*, 1997, 1145. (c) C. D. Hall, C. Suarez, H.-C. Anindita, A. N. A. Manu, C. D. Hall, G. J. Kirkovits and I. Ghiriviga, *Org. Biomol. Chem.*, 2003, **1**, 2973. (d) E. Biron, F. Otis, J.-C. Meillon, M. Robitaille, J. Lamothe, P. Van Hove, M.-E. Cormier and N. Voyer, *Bioorg. Med. Chem.*, 2004, **12**, 1279. (e) M. Yoshii, M. Yamamura, A. Satake and Y. Kobuke, *Org. Biomol. Chem.*, 2004, **2**, 2619. (f) P.-L. Boudreault and N. Voyer, *Org. Biomol. Chem.*, 2007, **5**, 1459.
8. M. R. Ghadiri, J. R. Granja and L. K. Buehler, *Nature*, 1994, **369**, 301.
9. H. S. Kim, J. D. Hartgerink and M. R. Ghadiri, *J. Am. Chem. Soc.*, 1998, **120**, 4417.
10. T. D. Clark, L. K. Buehler and M. R. Ghadiri, *J. Am. Chem. Soc.*, 1998, **120**, 651.
11. (a) R. Hourani, C. Zhang, R. van der Weegen, L. Ruiz, C. Li, S. Ketten, B. A. Helms and T. Xu, *J. Am. Chem. Soc.*, 2011, **133**, 15296. (b) L. Ruiz, A. Benjamin, M. Sullivan and S. Ketten, *J. Phys. Chem. Lett.* 2015, **6**, 1514.
12. (a) M. Amorín, L. Castedo and J. R. Granja, *Chem. Eur. J.*, 2008, **14**, 2100. (b) C. Reiriz, R. J. Brea, R. Arranz, J. L. Carrascosa, A. Garibotti, B. Manning, J. M. Valpuesta, R. Eritja, L. Castedo and J. R. Granja, *J. Am. Chem. Soc.*, 2009, **131**, 11335. (c) A. Guerra, R. J. Brea, M. Amorín, L. Castedo and J. R. Granja, *Org. Biomol. Chem.*, 2012, **10**, 8762. (d) J. Montenegro, C. Vázquez-Vázquez, A. Kalinin, K. E. Geckeler and J. R. Granja, *J. Am. Chem. Soc.*, 2014, **136**, 2484.
13. R. Garcia-Fandino, M. Amorin, L. Castedo and J. R. Granja, *Chem. Sci.*, 2012, **3**, 3280.
14. C. Reiriz, M. Amorin, R. Garcia-Fandino, L. Castedo and J. R. Granja, *Org. Biomol. Chem.*, 2009, **7**, 4358.
15. R. S. Kass, *J. Clin. Inves.*, 2005, **115**, 1986.
16. X. Hou, W. Guo, F. Xia, F.-Q. Nie, H. Dong, Y. Tian, L. Wen, L. Wang, L. Cao, Y. Yang, J. Xue, Y. Song, Y. Wang, D. Liu and L. Jiang, *J. Am. Chem. Soc.*, 2009, **131**, 7800. (b) X. Hou, F. Yang, L. Li, Y. Song, L. Jiang and D. Zhu, *J. Am. Chem. Soc.*, 2010, **132**, 11736. (c) R. Garcia-Fandino and M. S. P. Sansom, *Proc. Natl. Acad. Sci. USA*, 2012, **109**, 6939.
17. T. Jovanovic-Taliman, J. Tetenbaum-Novatt, A. S. McKenney, A. Zilman, R. Peters, M. P. Rout and B. T. Chait, *Nature*, 2009, **457**, 1023.
18. (a) A. Aksimentiev, *Nanoscale*, 2010, **2**, 468. (b) M. Fyta, S. Melchionna and S. Succi, *J. Polym. Sci. Part B: Polym. Phys.*, 2011, **49**, 985.
19. C. Maffeo, S. Bhattacharya, J. Yoo, D. Wells and A. Aksimentiev, *Chem. Rev.*, 2012, **112**, 6250.
20. (a) M. Engels, D. Bashford and M. R. Ghadiri, *J. Am. Chem. Soc.*, 1995, **117**, 9151. (b) M. Tarek, B. Maigret and C. Chipot, *Biophys. J.*, 2003, **85**, 2287. (c) H. Hwang, G. C. Schatz and M. A. Ratner, *J. Phys. Chem. B*, 2006, **110**, 26448. (d) H. Hwang, G. C. Schatz and M. A.

- Ratner, *J. Phys. Chem. B*, 2006, **110**, 6999. (e) C. Chipot and M. Tarek, *Phys. Biol.*, 2006, **3**, S20. (f) F. Dehez, M. Tarek and C. Chipot, *J. Phys. Chem. B*, 2007, **111**, 10633. (g) J. Zhu, J. Cheng, Z. Liao, Z. Lai, Z. and B. Liu, *J. Comput. Aided Mol. Des.*, 2008, **22**, 773. (h) J. Cheng, J. Zhu, B. Liu, Z. Liao and Z. Lai, *Mol. Simul.*, 2009, **35**, 625. (i) A. Khalfa, W. Treptow, B. Maigret and M. Tarek, *Chem. Phys.*, 2009, **358**, 161. (j) J. Liu, J. Fan, M. Tang and W. Zhou, *J. Phys. Chem. A*, 2010, **114**, 2376. (k) H. Liu, J. Chen, Q. Shen, W. Fu and W. Wu, *Mol. Pharmaceutics*, 2010, **7**, 1985. (l) R. Vijayaraj, S. V. Damme, P. Bultinck and V. Subramaniam, *J. Phys. Chem. B*, 2012, **116**, 9922.
21. (a) J. Cheng, J. Zhu and B. Liu, *Chem. Phys.*, 2007, **333**, 105. (b) R. Garcia-Fandino, J. R. Granja, D. A. Marco and M. Orozco, *J. Am. Chem. Soc.*, 2009, **131**, 15678. (c) R. García-Fandiño and J. R. Granja, *J. Phys. Chem. C.*, 2013, **117**, 10143.
22. M. Amorin, L. Castedo and J. R. Granja, *J. Am. Chem. Soc.*, 2003, **125**, 2844.
23. R. Garcia-Fandino, L. Castedo, J. R. Granja and S. Vázquez, *J. Phys. Chem. B*, 2010, **114**, 4973.
24. (a) J. Wang, W. Wang, P. A. Kollman and D. A. Case, *J. Mol. Graphics Modell*, 2006, **25**, 247. (b) J. Wang, R. M. Wolf, J. W. Caldwell, P. A. Kollman and D. A. Case, *J. Comput. Chem.*, 2004, **25**, 1157. (c) J. Wang, R. M. Wolf, J. W. Caldwell, P. A. Kollman and D. A. Case, *J. Comput. Chem.*, 2004, **25**, 1157.
25. I. S. Joung and T. E. Cheatham, *J. Phys. Chem. B*, 2008, **112**, 9020.
26. D. A. Case, T. A. Darden, T. E. Cheatham, C. L. Simmerling, J. Wang, R. E. Duke, R. Luo, M. Crowley, R. C. Walker, W. Zhang, K. M. Merz, B. Wang, S. Hayik, A. Roitberg, G. Seabra, I. Kilossváry, K. F. Wong, F. Paesani, J. Vanicek, X. Wu, S. R. Brozell, T. Steinbrecher, H. Gohlke, L. Yang, C. Tan, J. Mongan, V. Hornak, G. Cui, D. H. Mathews, M. G. Seetin, C. Sagui, V. Babin and P. A. Kollman, AMBER 10, University of California, San Francisco, 2008.
27. S. W. I. Siu, R. Vacha, P. Jungwirth and R. A. Böckmann, *J. Chem. Phys.*, 2008, **128**, 125103/1. The structure of the membrane was downloaded from <http://www.bioinf.uni-sb.de/RB>
28. B. Hess, C. Kutzner, D. van der Spoel and E. Lindahl, *J. Chem. Theory Comput.*, 2008, **4(3)**, 435.
29. M. Parrinello and A. Rahman, *J. Appl. Phys.*, 1981, **52**, 7182.
30. G. Bussi, D. Donadio and M. Parrinello, *J. Chem. Phys.*, 2007, **126**, 014101.
31. B. Hess, H. Bekker, H. J. C. Berendsen and G. J. E. M. Fraaije, *J. Comput. Chem.*, 1997, **18**, 1463.
32. U. Essman, L. Perera, M. Berkowitz, T. Darden, H. Lee, L. Pedersen, *J. Chem. Phys.*, 1995, **103**, 8577.
33. (a) S. Kumar, J. M. Rosenberg, D. Bouzida, R. H. Swendsen and P. A. Kollman, *J. Comput. Chem.*, 1995, **16**, 1339. (b) A. Grossfield, An implementation of WHAM: the weighted histogram analysis method, <http://membrane.urmc.rochester>.

- edu/Software/WHAM/WHAM.html (c) Sm. Kumar, D. Bouzida, R. H. Swendsen, P. A. Kollman and J. M. Rosenberg, *J. Comput. Chem.*, 2002, **13**, 1011.
34. W. Humphrey, A. Dalke and K. Schulten, *J. Mol. Graphics*, 1996, **14**, 33.
35. O. Beckstein and M. S. P. Sansom, *Phys. Biol.*, 2004, **1**, 42.
36. O. S. Smart, J. G. Neduvilil, X. Wang, B. A. Wallace and M. S. P. Sansom, *J. Mol. Graph.*, 1996, **14**, 354.
37. (a) E. Gouaux and R. Mackinnon, *Science*, 2005, **310**, 1461. (b) B. Roux, S. Berneche, B. Egwolf, B. Lev, S. Y. Noskov, C. N. Rowley and H. Yu, *J. Gen. Physiol.*, 2011, **137**, 415. (c) B. Alberts, D. Bray, J. Lewis, M. Raff, K. Roberts and J. Watson, *Molecular Biology of the Cell*, Garland Publishing, Inc., New York, 3rd edn, 1994.
38. (a) A. Alexiadis and S. Kassinos, *Chem. Rev.*, 2008, **108**, 5014. (b) J. C. Rasaiah, S. Garde and G. Hummer, *Annu. Rev. Phys. Chem.*, 2008, **59**, 713.
39. (a) R. Lynden-Bell and J. C. Rasaiah, *J. Chem. Phys.*, 1996, **105**, 9266. (b) S. Koneshan, J. C. Rasaiah, R. M. Lynden-Bell and S. H. Lee, *J. Phys. Chem. B.*, 1998, **102**, 4193.
40. (a) S. Obst and H. Bradaczek, *J. Phys. Chem.*, 1996, **100**, 15677. (b) V. Mile, L. Pusztai, H. Dominguez and O. Pizio, *J. Phys. Chem. B*, 2009, **113**, 10760.
41. L. Tang, T. M. GAmal El-Din, J. Payandeh, G. Q. Martinez, T. M. Heard, T. Scheuer, N. Zheng and W. A. Catterall, *Nature*, 2014, **505**, 56.
42. (a) B. Corry, *PeerJ* *1.*, 2013, e16. (b) N. Chakrabarti, C. Ing, J. Payandeh, N. Zheng, W. A. Catterall, *Proc. Natl. Acad. Sci. USA*, 2013, **110**, 11331 and references therein.
43. N. Rodríguez-Vázquez, S. Salzinger, L. F. Silva, M. Amorín and J. R. Granja, *Eur. J. Org. Chem.*, 2013, 3477.